Thermochemical Studies of Pyrazolide†

Adam J. Gianola, Takatoshi Ichino, Shuji Kato, Veronica M. Bierbaum,* and W. Carl Lineberger*

JILA, University of Colorado and National Institute of Standards and Technology and Department of Chemistry and Biochemistry, University of Colorado, Boulder, Colorado 80309-0440

Received: December 24, 2005; In Final Form: February 14, 2006

The 351.1 nm photoelectron spectrum of 1-pyrazolide anion has been measured. The 1-pyrazolide ion is produced by hydroxide (HO^-) deprotonation of pyrazole in a flowing afterglow ion source. The electron affinity (EA) of the 1-pyrazolyl radical has been determined to be 2.938 ± 0.005 eV. The angular dependence of the photoelectrons indicates near-degeneracy of low-lying states of 1-pyrazolyl. The vibronic feature of the spectrum suggests significant nonadiabatic effects in these electronic states. The gas phase acidity of pyrazole has been determined using a flowing afterglow-selected ion flow tube; $\Delta_{acid}G_{298} = 346.4 \pm 0.3$ kcal mol^{-1} and $\Delta_{acid}H_{298} = 353.6 \pm 0.4$ kcal mol^{-1}. The N−H bond dissociation energy (BDE) of pyrazole is derived to be D_0(pyrazole, N−H) = 106.4 ± 0.4 kcal mol^{-1} from the EA and the acidity using a thermochemical cycle. In addition to 1-pyrazolide, the photoelectron spectrum demonstrates that HO^- deprotonates pyrazole at the C5 position to generate a minor amount of 5-pyrazolide anion. The photoelectron spectrum of 5-pyrazolide has been successfully reproduced by a Franck−Condon (FC) simulation based on the optimized geometries and the normal modes obtained from B3LYP/6-311++G(d,p) electronic structure calculations. The EA of the 5-pyrazolyl radical is 2.104 ± 0.005 eV. The spectrum exhibits an extensive vibrational progression for an in-plane CCN bending mode, which indicates a substantial difference in the CCN angle between the electronic ground states of 5-pyrazolide and 5-pyrazolyl. Fundamental vibrational frequencies of 890 ± 15, 1110 ± 35, and 1345 ± 30 cm^{-1} have been assigned for the in-plane CCN bending mode and two in-plane bond-stretching modes, respectively, of $\tilde{X}\ ^2A'$ 5-pyrazolyl. The physical properties of the pyrazole system are compared to the isoelectronic systems, pyrrole and imidazole.

Introduction

Nitrogen-rich compounds have recently attracted attention as high-energy-density materials.[1−6] To better understand their nature, we have initiated a systematic investigation of nitrogen-containing, five-membered heterocyclic compounds and their deprotonated ions. Our main goal is to elucidate how the physical properties of the heterocyclic compounds change as the number of N atoms in the five-membered ring increases. We have previously reported our studies on pyrrole,[7] which has one N atom in the ring, and imidazole,[8] which has two N atoms. Discussion was presented regarding the effects of the additional N atom on properties such as the acidities and bond dissociation energy (BDE) of imidazole, and the electron binding energy (eBE) of the deprotonated ion, imidazolide, compared to the pyrrole system.[8] In the present paper, we report our study on the thermodynamic properties of pyrazole, a structural isomer of imidazole.

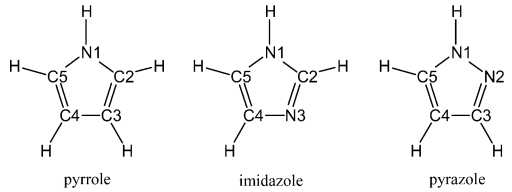

In pyrazole, two N atoms are directly bonded to each other. It is not obvious how the difference in molecular structure between pyrazole and imidazole brings about differences in various physical properties. We have carried out photoelectron spectroscopic measurements on 1-pyrazolide (i.e., pyrazole deprotonated at the N atom)[9] to determine the electron affinity (EA) of the 1-pyrazolyl radical. We have also measured the rate constants of the proton transfer reactions for pyrazole and pyrazolide to determine the gas phase acidity of pyrazole. These parameters are combined in a negative ion thermochemical cycle to derive the N−H BDE of pyrazole. Additionally, we have also observed the photoelectron spectra of a carbon-deprotonated ion, 5-pyrazolide, a minor product ion of the reaction of hydroxide ion (HO^-) with pyrazole.

We first present the photoelectron spectrum of 1-pyrazolide and the spectral analysis. We have found the importance of nonadiabatic effects in the low-lying states of 1-pyrazolyl, which will be described in detail in a separate paper.[10] The photoelectron spectrum of 5-pyrazolide and its analysis will be given next. The following section provides the results of our gas phase acidity measurements for pyrazole using a flowing afterglow-selected ion flow tube (FA-SIFT) instrument. After the presentation of our experimental studies, the thermodynamic properties of the pyrazole system will be discussed, as well as the electronic structure of the corresponding radicals.

Experimental Methods

Negative Ion Photoelectron Spectroscopy. Ultraviolet negative ion photoelectron spectra have been obtained with a photoelectron spectrometer, as described in detail elsewhere.[11−13] Atomic oxygen anion (O^-) is generated by seeding a trace

† Part of the "Chava Lifshitz Memorial Issue".

* To whom correspondence should be addressed. E-mail: veronica.bierbaum@colorado.edu (V.M.B.); wcl@jila.colorado.edu (W.C.L.).

10.1021/jp057499+ CCC: $33.50
Published on Web 03/16/2006

amount of O_2 in approximately 0.5 Torr of helium in a microwave discharge flowing afterglow ion source. The O^- reacts with methane introduced downstream to produce hydroxide ion (HO^-). Pyrazole ($C_3H_4N_2$, Aldrich, 98%) is introduced further downstream by flowing a stream of helium through a crystalline sample. Deprotonation of pyrazole by HO^- generates pyrazolide ions ($C_3H_3N_2^-$). In some measurements, O^- and fluoride ion (F^-), generated from NF_3 in the discharge source, have also been used as deprotonation agents. Collisions with the helium buffer gas in the flow tube thermalize the ions to a temperature of ~298 K. Alternatively, the jacket surrounding the flow tube is filled with liquid nitrogen to allow for additional cooling to ~200 K. The anions are extracted from the flowing afterglow region, accelerated to 736 eV, and focused into a Wien velocity filter for mass selection. The mass-selected ions are refocused, decelerated to 35 eV, and crossed with a photon beam from a continuous wave (CW) argon ion laser (351.1 nm; 3.531 eV) in an external build-up cavity with a circulating power of approximately 100 W. A typical beam current is ~200 pA for pyrazolide synthesized at room temperature.

Photoelectrons collected in a direction perpendicular to the ion and laser beams are focused, passed through a hemispherical energy analyzer with 8−10 meV resolution, and imaged onto a position sensitive detector after amplification with microchannel plates. Spectra are obtained by measuring photoelectron counts as a function of electron kinetic energy (eKE), and eKE is converted to electron binding energy (eBE) by subtracting the eKE from the photon energy. For the analysis of the 1-pyrazolide spectrum, the absolute kinetic energy is calibrated with the known electron affinity (EA) of the iodine atom[14,15] in the measurements of the photoelectron spectrum of the iodide anion (I^-). In the case of the 5-pyrazolide spectrum, where the photoelectrons have higher kinetic energies, O^- is used for the calibration. A small energy compression factor[11] is corrected for as determined through photoelectron spectrum measurements of sulfur anion (S^-) in addition to O^- and I^-. A rotatable half-wave plate is inserted into the laser path before the build-up cavity to change the angle (θ) between the electric field vector of the laser beam and the photoelectron collection axis. Photoelectrons have angular distributions according to[16]

$$I(\theta) = \frac{\sigma_0}{4\pi}(1 + \beta P_2(\cos\theta)) \quad (1)$$

where σ_0 is the total photodetachment cross section, β is the anisotropy parameter, and $P_2(\cos\theta)$ is the second Legendre polynomial. Measurements at the magic angle (54.7°) provide spectra free from the angular dependence. The anisotropy parameter is determined by measurements of the photoelectron counts at $\theta = 0$ and 90°.

Flowing Afterglow-Selected Ion Flow Tube (FA-SIFT) Measurements. The gas phase acidity of pyrazole has been measured using a tandem FA-SIFT instrument that has been described previously.[17,18] To establish the acidity of pyrazole, the forward (k_f) and reverse (k_r) rate constants are measured at 298 K for proton transfer reactions between pyrazole ($C_3H_4N_2$) and a reference acid, 2-methyl-2-propanethiol ($(CH_3)_3CSH$). The ratio of the rate constants gives the proton transfer equilibrium constant ($K_{equil} \equiv k_f/k_r$).

$$C_3H_3N_2^- + (CH_3)_3CSH \underset{k_r}{\overset{k_f}{\rightleftharpoons}} C_3H_4N_2 + (CH_3)_3CS^- \quad (2)$$

The reactant anions [$C_3H_3N_2^-$ or $(CH_3)_3CS^-$] are generated in the source flow tube using HO^- deprotonation of the corresponding neutrals. The ions are mass selected and injected into the second flow tube at low injection energies in order to minimize fragmentation. The reactant anions are thermally equilibrated with the helium buffer gas (0.5 Torr) before undergoing proton transfer reactions with a neutral reagent added in the second flow tube. For the forward reaction, $(CH_3)_3CSH$ is added through each of the multiple inlets located downstream along the flow tube. Depletion of the reactant ion signal is recorded with the detection quadrupole mass filter as a function of the inlet position (i.e., the reaction distance) and reaction rates are determined.[17,18] For the reverse reaction, a solid sample of pyrazole is heated to about 50 °C and sublimed into a stream of helium, which is then introduced into the SIFT flow tube for the subsequent reaction with $(CH_3)_3CS^-$. From alternate measurements of semilogarithmic depletions of SIFT-injected HO^- and $(CH_3)_3CS^-$ in the constant pyrazole flow, the pyrazole concentration is calibrated assuming a 90% efficiency (with respect to the calculated collision rate constant, 3.37×10^{-9} $cm^3\ s^{-1}$) for the proton transfer reaction between pyrazole and HO^-, and the rate constant for the $(CH_3)_3CS^-$ reaction with pyrazole is determined. This calibration procedure is the same as that used previously for imidazole.[8] The parametrized trajectory collision rate theory[19] is used to calculate the collision rate constant for the HO^- reaction with pyrazole, whose polarizability[20] and electric dipole moment[21] are 7.15×10^{-24} cm^3 and 2.20 D, respectively. Using the acidity of 2-methyl-2-propanethiol,[8,22−24] $\Delta_{acid}G_{298}[(CH_3)_3CSH] = 346.2 \pm 0.2$ kcal mol^{-1}, the acidity of pyrazole is determined from the equilibrium constant via the expression

$$\Delta_{acid}G_{298}(\text{pyrazole}) = \Delta_{acid}G_{298}[(CH_3)_3CSH] + RT\ln K_{equil} \quad (3)$$

Gas phase acidity bracketing measurements have been performed to examine the identity of the SIFT-injected ion, $C_3H_3N_2^-$, using $(CH_3)_3CSH$ and CH_3SH ($\Delta_{acid}G_{298} = 351.6 \pm 0.4$ kcal mol^{-1}).[7] The anion has been confirmed to be almost exclusively 1-pyrazolide, as explained below in the Results section.

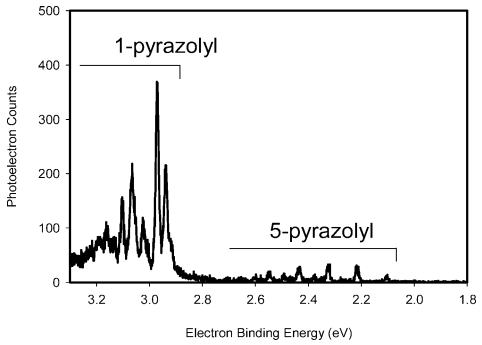

Figure 1. Magic angle photoelectron spectrum (351.1 nm) of *m*/*z* 67 ions produced from the HO^- reaction with pyrazole in the flow tube at room temperature.

Results

Photoelectron Spectra: 1-Pyrazolide. Figure 1 shows the magic angle photoelectron spectrum of *m*/*z* ~67 ions produced from the HO^- reaction with pyrazole. Intense peaks are observed at eBE > 2.9 eV, along with several weak peaks at eBE < 2.6 eV. We also measured photoelectron spectra of *m*/*z* ~67 ions generated from the O^- and F^- reactions with pyrazole. The spectra obtained with these reactant ions are virtually identical with that in Figure 1 at eBE > 2.9 eV, but there are no

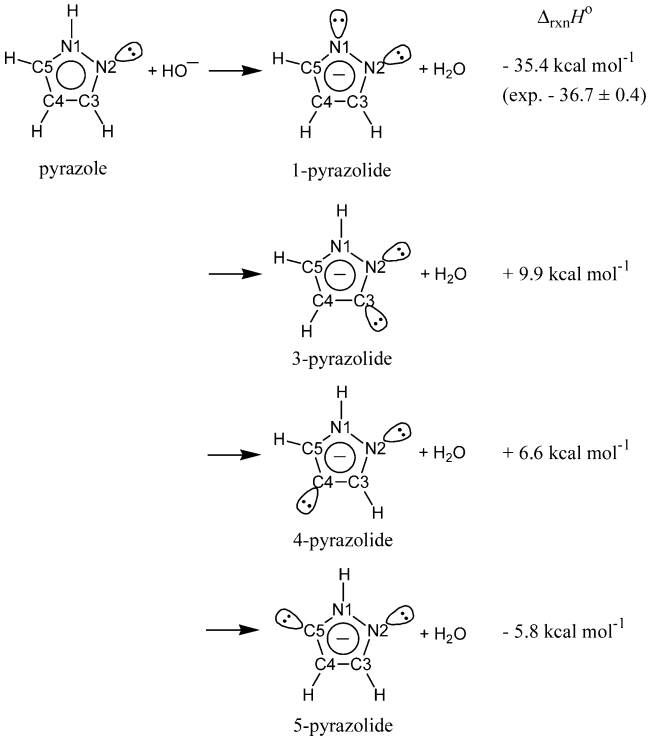

Figure 2. Reaction enthalpies evaluated for HO^- deprotonation of pyrazole at different positions. The enthalpies of pyrazole and pyrazolides are evaluated from the B3LYP/6-311++G(d,p) calculations, while the deprotonation enthalpy of H_2O is from ref 24.

photoelectron signals observed at the lower eBE. The beam current of the m/z ~67 ions obtained with O^- or F^- reagents is comparable to that when HO^- is used.

These observations are reminiscent of those made when we measured the photoelectron spectra of imidazolide.[8] The HO^- is sufficiently basic such that imidazole can be deprotonated also at the C5 position, leading to the formation of 5-imidazolide ions, even though the majority of HO^- ions abstract the most acidic proton at the N atom, producing 1-imidazolide ions. The identity of 5-imidazolide was positively confirmed through Franck−Condon fitting of the corresponding photoelectron spectrum. The proton at the C5 position of imidazole is far less acidic than that at the N atom, and 5-imidazolide photoelectron signals are not detected when O^-, which is a less basic deprotonating agent than HO^-, is used to generate m/z 67 ions.

Electronic structure calculations were performed to explore the acidities of pyrazole, using density functional theory (DFT). The variation of DFT employed is Becke's hybrid three-parameter functional[25] and the correlation functional of Lee, Yang, and Parr[26] (i.e., B3LYP), with the 6-311++G(d,p) basis set.[27] The calculations were implemented with the Gaussian 03 program package.[28] Figure 2 shows the reaction enthalpies evaluated for the HO^- deprotonation of pyrazole to produce pyrazolide isomers. The results of the DFT calculations for pyrazole and all of the pyrazolides were combined with an experimental value of the deprotonation enthalpy of H_2O ($\Delta_{acid}H_{298}$ = 390.27 ± 0.03 kcal mol^{-1})[24] to derive the reaction enthalpies. The DFT harmonic vibrational frequencies were used without scaling in the evaluation of thermodynamic parameters throughout the present study. Deprotonation at the N atom, forming 1-pyrazolide, is the most exothermic process, with a reaction enthalpy of −35.4 kcal mol^{-1}. This value is in good agreement with the experimental value −36.7 ± 0.4 kcal mol^{-1} (see below). For deprotonation at the carbon sites, only the 5-pyrazolide formation is predicted to be exothermic, with a reaction enthalpy of −5.8 kcal mol^{-1}. When O^- ($\Delta_{acid}H_{298}$(OH) = 382.60 ± 0.07 kcal mol^{-1})[29] or F^- ($\Delta_{acid}H_{298}$(HF) = 371.331 ± 0.003 kcal mol^{-1})[24] is used, deprotonation at the C5 position becomes endothermic. This DFT study suggests that the weak photoelectron signals observed at eBE < 2.6 eV in Figure 1 may represent detachment from 5-pyrazolide, produced in a minor pathway of the HO^- reaction with pyrazole, while the intense peaks at the higher eBE may originate from 1-pyrazolide, the major product of the HO^- reaction.

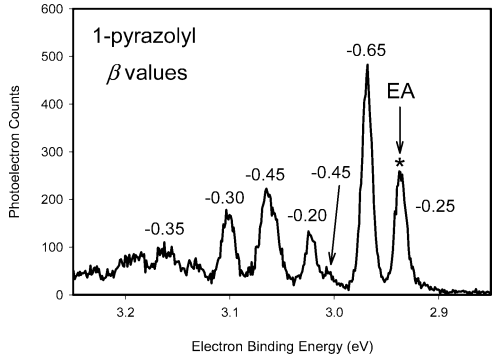

Figure 3. Magic angle photoelectron spectrum (351.1 nm) of 1-pyrazolide produced from the HO^- deprotonation of pyrazole in the flow tube cooled with liquid nitrogen. The peak marked with an asterisk is the origin peak of the electronic ground state of the 1-pyrazolyl radical. The values in the figure represent the anisotropy parameters (β) for the corresponding peaks.

TABLE 1: B3LYP/6-311++G(d,p) Optimized Geometries for 1-Pyrazolide and 1-Pyrazolyl[a]

	1-pyrazolide	1-pyrazolyl		
	$\tilde{X}\ ^1A_1$	$\tilde{X}\ ^2A_2$	$\tilde{A}\ ^2B_1$	$\tilde{B}\ ^2B_2$
N1−N2	1.3621	1.2750	1.4676	1.2396
N2−C3 (N1−C5)	1.3491	1.4300	1.2991	1.3577
C3−C4 (C4−C5)	1.4044	1.3861	1.4374	1.4051
C3−H (C5−H)	1.0853	1.0805	1.0816	1.0759
C4−H	1.0824	1.0773	1.0813	1.0789
∠N1−N2−C3 (∠N2−N1−C5)	107.89	108.34	107.53	111.54
∠N2−C3−C4 (∠N1−C5−C4)	110.85	109.98	110.96	105.72
∠C3−C4−C5	102.52	103.36	103.02	105.48
∠N2−C3−H (∠N1−C5−H)	120.36	119.63	121.39	122.04
∠C3−C4−H (∠C5−C4−H)	128.74	128.32	128.49	127.26

[a] Bond lengths are in units of angstroms, and bond angles are in units of degrees.

Figure 3 shows a higher eBE portion of the magic angle photoelectron spectrum of m/z ~67 ions produced from the reaction of HO^- with pyrazole. This spectrum was taken with the same experimental conditions as those used for the spectrum in Figure 1 except that the flow tube was cooled with liquid N_2, such that there are fewer contributions from vibrationally (and rotationally) hot ions in Figure 3. Intuitively, among all of the peaks observed, the one at the lowest eBE (marked with an asterisk in Figure 3) is expected to be the vibrational origin of the electronic ground state of the 1-pyrazolyl radical. DFT calculations were performed to derive the EA of 1-pyrazolyl. C_{2v} symmetry was found for the optimized geometries of the electronic ground states of both 1-pyrazolide ($^1A_1$) and 1-pyrazolyl ($^2A_2$). Table 1 shows the optimized geometries from the DFT calculations. The DFT-predicted EA is 2.945 eV. With the peak marked with an asterisk in Figure 3 assigned as the vibrational origin, the experimental EA is 2.938 ± 0.005 eV. The DFT prediction of the 1-pyrazolyl EA is in good agreement with the experimental results, and we adopt this assignment of the vibrational origin. Accurate EA predictions by DFT calcula-

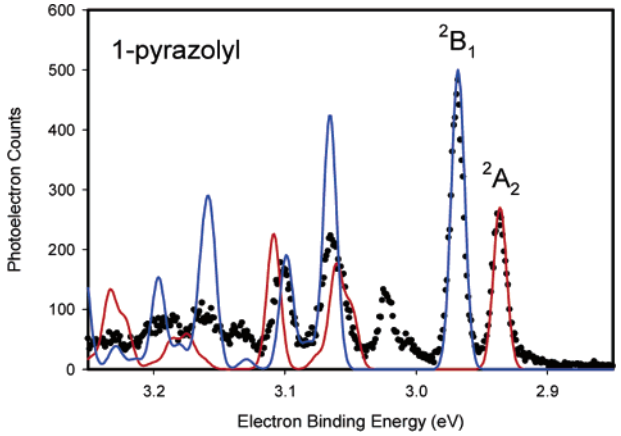

Figure 4. Franck−Condon simulation of the magic angle photoelectron spectrum of 1-pyrazolide from Figure 3 (dots). The red and blue lines are the simulated spectra for the detachment to the $^2A_2$ and $^2B_1$ states, respectively, of the 1-pyrazolyl radical. The simulation used the optimized geometries and normal modes obtained from the B3LYP/6-311++G(d,p) calculations.

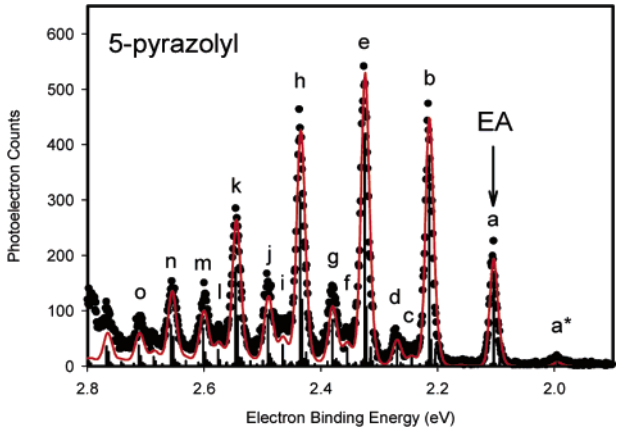

Figure 5. Magic angle photoelectron spectrum (351.1 nm) of 5-pyrazolide produced from the HO^- deprotonation of pyrazole in a flow tube at room temperature (dots). The red line is the Franck−Condon simulation of the spectrum based on the optimized geometries and normal modes obtained from the B3LYP/6-311++G(d,p) calculations. The sticks represent the transitions to the individual vibrational levels of $\tilde{X}\ ^2A'$ 5-pyrazolyl.

tions have also been observed for the isoelectronic systems, that is, 1-pyrrolyl radical[7] and 1-imidazolyl radical.[8]

Anisotropy parameters (β) for the observed peaks are given in Figure 3. The most intense peak, observed at 32 ± 1 meV above the origin peak, has $\beta = -0.65$, which is significantly different from that of the origin peak, $\beta = -0.25$. Observation of distinct anisotropy parameters indicates detachment from different molecular orbitals of the anion, that is, access to different electronic states of the neutral. DFT calculations were performed to study the electronic states of different electronic symmetry. The lowest excited state of 1-pyrazolyl is predicted to be the $^2B_1$ state, with a term energy of only 31 meV. The optimized geometry of the $^2B_1$ state can be found in Table 1. The good agreement between the experimental observation and the DFT term energy may be fortuitous. However, the agreement between the experiment and the DFT calculations is excellent in that both indicate near-degeneracy of the ground state and the first excited state.

To further aid in the assignments of the photoelectron spectra, Franck−Condon (FC) simulation was performed based on the DFT optimized geometries (Table 1) and normal modes of the anion and neutral states, using the PESCAL program.[30,31] The DFT harmonic frequencies are provided in the Supporting Information. Figure 4 shows the results of the FC simulation, superimposed on the experimental spectrum (dots) from Figure 3. The FC factors were calculated for the transitions from the anion ground state ($^1A_1$) to the neutral ground state ($^2A_2$) as well as to the first excited state ($^2B_1$).[32] Convolution with a Gaussian function of 15 meV full width at half-maximum (fwhm) was applied to the FC factors. The red line in Figure 4 represents the transition to the $^2A_2$ state, while the transition to the $^2B_1$ state is represented by the blue line. The eBE positions of the origin peaks of the two simulated spectra have been slightly adjusted to match the corresponding experimental origin peak positions. Also, the intensities of the two simulated spectra have been normalized to those of the corresponding experimental origin peaks. For the present purpose, no contribution from vibrationally excited levels of the electronic ground state of the anion was taken into account in the simulation. As apparent in Figure 4, agreement between the FC simulation and the experimentally observed spectra is generally poor. The band with moderate intensity observed about 50 meV above the $^2B_1$ origin peak is completely missed by the FC simulation. Also, the intensity of the bands at the higher eBE is severely overestimated.[33] This disagreement is surprising, since the FC simulation of the transition from the anion to the neutral ground states has been found to successfully reproduce the photoelectron spectra of the isoelectronic systems, that is, 1-pyrrolide[7] and 1-imidazolide.[8] Switching of the assignments of the two neutral states (i.e., $^2B_1$ as the ground state and $^2A_2$ as the excited state) does not alleviate the disagreement.

We have found that the failure of the FC fitting is due mainly to a pseudo-Jahn−Teller vibronic coupling between the low-lying states. We have carried out a simulation of the 1-pyrazolide spectrum by establishing a diabatic model Hamiltonian[34−36] for the neutral states around the equilibrium geometry of the anion ground state. This model Hamiltonian takes into account the nonadiabatic effects, which are neglected in the FC simulation in Figure 4. Parametrization of the model Hamiltonian has been accomplished with ab initio calculations using the equation-of-motion coupled cluster theory (EOMIP-CCSD).[37,38] The simulation reproduces the observed spectrum very well and confirms that our assignment of the origin peak is correct. Details of this simulation procedure as well as the results of the simulation will be presented in a forthcoming paper.[10]

Photoelectron Spectra: 5-Pyrazolide. As explained in the preceding section, the lower eBE portion of the spectrum in Figure 1 is most probably attributed to detachment from 5-pyrazolide. Figure 5 shows the magic angle photoelectron spectrum (dots) in the lower eBE region for m/z ~67 ions produced from the HO^- reaction with pyrazole. The experimental conditions used for the measurements of the spectrum in Figure 5 are virtually identical to those in Figure 1. Table 2 shows the observed peak positions in Figure 5 relative to peak a. DFT calculations were carried out to obtain the optimized geometries and the harmonic frequencies of the anion and neutral ground states. The calculations found minima in C_s symmetry for the electronic ground states of both 5-pyrazolide anion ($^1A'$) and 5-pyrazolyl radical ($^2A'$). The optimized geometries are provided in Table 3. FC simulation was performed for the transition from $\tilde{X}\ ^1A'$ 5-pyrazolide to $\tilde{X}\ ^2A'$ 5-pyrazolyl, using the results of the DFT calculations. The DFT harmonic frequencies are available in the Supporting Information. The red line in Figure 5 is the result of the FC simulation, which utilized a vibrational temperature of 298 K for the anion. The agreement with the experimental spectrum is very good.

TABLE 2: Peak Positions and Assignments for the Photoelectron Spectrum of 5-Pyrazolide

peak[a]	peak position[b] (cm^{-1})	assignment[c]
a*[d]	880 ± 20	13_1^0
a	0	0_0^0
b	890 ± 15	12_0^1
c	1110 ± 35	9_0^1
d	1345 ± 30	6_0^1
e	1780 ± 20	12_0^2
f	1990 ± 35	$9_0^1 12_0^1$
g	2225 ± 35	$6_0^1 12_0^1$
h	2665 ± 25	12_0^3
i	2990 ± 50	$9_0^1 12_0^2$
j	3115 ± 25	$6_0^1 12_0^2$
k	3555 ± 35	12_0^4
l	3790 ± 35	$9_0^1 12_0^3$
m	4000 ± 45	$6_0^1 12_0^3$
n	4440 ± 35	12_0^5
o	4880 ± 35	$6_0^1 12_0^4$

[a] Peak labels used in Figure 5. [b] Relative to the origin (peak a). [c] The ν_6 mode is CCC asymmetric stretching, ν_9 is ring breathing, and ν_{12} is CCN bending for $\tilde{X}\ ^2A'$ 5-pyrazolyl. All of these modes are a′ modes in C_s symmetry. Significant contributions from another in-plane bending mode (the ν_{13} mode of the radical) are noticeable in Franck−Condon fitting of the peaks with higher vibrational quanta (see the text). [d] A vibrational hot band for an in-plane CCN bending mode (ν_{13}) of $\tilde{X}\ ^1A'$ 5-pyrazolide.

TABLE 3: B3LYP/6-311++G(d,p) Optimized Geometries for 5-Pyrazolide and 5-Pyrazolyl[a]

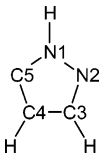

	$\tilde{X}\ ^1A'$ 5-pyrazolide	$\tilde{X}\ ^2A'$ 5-pyrazolyl
N1−N2	1.3804	1.3630
N2−C3	1.3350	1.3326
C3−C4	1.4144	1.4172
C4−C5	1.4177	1.3737
C5−N1	1.3707	1.3403
N1−H	1.0058	1.0064
C3−H	1.0855	1.0801
C4−H	1.0835	1.0760
∠N1−N2−C3	101.71	104.43
∠N2−C3−C4	111.66	112.77
∠C3−C4−C5	108.48	102.17
∠C4−C5−N1	100.08	109.82
∠C5−N1−N2	118.06	110.81
∠H−N1−N2	116.55	119.91
∠N2−C3−H	118.90	119.11
∠C5−C4−H	125.60	128.52

[a] Bond lengths are in units of angstroms, and bond angles are in units of degrees.

The sticks in Figure 5 represent the positions and relative intensities of transitions to the individual vibrational levels of $\tilde{X}\ ^2A'$ 5-pyrazolyl. The FC fitting positively identifies peak a in Figure 5 as the vibrational origin of $\tilde{X}\ ^2A'$ 5-pyrazolyl. Thus, the EA of 5-pyrazolyl is determined to be 2.104 ± 0.005 eV. The DFT calculations predict the EA of 5-pyrazolyl to be 2.109 eV, in excellent agreement with the experimental value. It should be noted that the position of the origin peak of the simulated spectrum in Figure 5 has been slightly adjusted to match the experimental peak position. The DFT calculations predict that the EAs of 3-pyrazolyl and 4-pyrazolyl are 1.337 and 1.618 eV, respectively. Also, the FC profiles for the transitions from the ground states of 3-pyrazolide and 4-pyrazolide to the corresponding neutral ground states are quite different from that in Figure 5. Thus, it is concluded that a portion of HO^- ions deprotonate pyrazole at the C5 position, and the photodetachment from 5-pyrazolide accounts for the observation of the spectrum shown in Figure 5.

The most conspicuous feature of the spectrum is the intense peaks with a constant energy spacing (peaks b, e, h, k, and n). The FC fitting indicates that these peaks represent the vibrational progression along an in-plane mode (a′) of CCN bending motion centered at C5 (ν_{12}, see the Supporting Information). The optimized geometry of the 5-pyrazolide ground state has a C4−C5−N1 angle of 100.1°, while it is 109.8° in the 5-pyrazolyl ground state (Table 3). Thus, upon photodetachment, the CCN bending motion is activated, which appears as the extensive vibrational progression in Figure 5. The position of peak b gives a fundamental vibrational frequency of 890 ± 15 cm^{-1} for this CCN bending mode. The DFT harmonic frequency for this mode was calculated to be 915 cm^{-1}. For presentation purposes, the FC simulation in Figure 5 used a frequency scaling factor of 0.975 for all modes,[39] in order to match the DFT frequency to the experimental fundamental frequency for the CCN bending mode. It is evident that the FC fitting is excellent even at a vibrational quantum number of 5 (peak n), corroborating the harmonic assumption used in the FC simulation for this particular mode. It should be mentioned, however, that there is another in-plane ring bending mode which is moderately active in the FC simulation. This mode has a DFT harmonic frequency of 886 cm^{-1} (ν_{13}, see the Supporting Information). The energy separation between this mode and the CCN bending mode is too small to be resolved in our photoelectron measurements. According to the FC simulation, contribution of the ν_{13} mode is negligible in peaks b and e, but it becomes more significant for peaks with higher vibrational quanta.

There are two other a′ modes noticeable in Figure 5. Peak c is the fundamental level of the ν_9 mode, and peak d is the fundamental level of the ν_6 mode. The ν_9 mode represents ring breathing motion, while the ν_6 mode represents CCC asymmetric stretching. The fundamental vibrational frequencies were determined to be 1110 ± 35 and 1345 ± 30 cm^{-1} for the ν_9 and ν_6 modes, respectively (Table 2). Peaks c, f, i, and l are a vibrational progression of the ν_{12} mode off the fundamental level of the ν_9 mode. Similarly, peaks d, g, j, m, and o are a vibrational progression of the ν_{12} mode off the fundamental level of the ν_6 mode. A vibrational hot band (peak a*) is also observed in the spectrum. The FC simulation indicates that this hot band should be assigned to the fundamental level (880 ± 20 cm^{-1}) of an in-plane CCN bending mode (ν_{13}) of $\tilde{X}\ ^1A'$ 5-pyrazolide.

The anisotropy parameter (β) is 0.35 for the peaks in Figure 5.

Gas Phase Acidity. For reactions of 1-pyrazolide with $(CH_3)_3CSH$ and pyrazole with $(CH_3)_3CS^-$ (eq 2), the overall rate constants ($k_{overall}$) including proton transfer and adduct formation were measured to be (1.10 ± 0.22) × 10^{-9} and (7.9 ± 2.1) × 10^{-10} $cm^3\ s^{-1}$, respectively. The uncertainty in the forward rate constant comes from an absolute error bar in the standard kinetics measurements (±20%), while there is an additional uncertainty for the reverse reaction due to the calibration of pyrazole concentration (see the Experimental Section). The reaction of 1-pyrazolide with $(CH_3)_3CSH$ is faster than the reverse reaction, indicating that the forward direction is exoergic in the proton transfer equilibrium. This is consistent with the observed branching fractions for proton transfer versus

adduct formation; the reaction of 1-pyrazolide with $(CH_3)_3CSH$ proceeds almost exclusively via proton transfer (≈98%), whereas the reverse reaction produces more adducts (≈91% proton transfer). The overall rate constants can be partitioned to derive the effective rate constants for proton transfer, with the reasonable assumption that the adduct formation arises from the fraction of the ion−molecule complexes that are endoergic with respect to proton transfer. Thus, the rate constants for proton transfer reactions in eq 2 are $k_f = (1.08 \pm 0.22) \times 10^{-9}$ $cm^3\ s^{-1}$ and $k_r = (7.2 \pm 1.9) \times 10^{-10}\ cm^3\ s^{-1}$. With these values used in eq 3, the gas phase acidity $[\Delta_{acid}G_{298}(pyrazole)]$ is determined to be 346.4 ± 0.3 kcal mol^{-1}. This experimental value of the gas phase acidity of pyrazole is in excellent agreement with a previous measurement[40,41] of 346.4 ± 2.0 kcal mol^{-1} after inclusion of recent changes in the acidity scale.[42]

As mentioned in a previous section, the reaction of HO^- with pyrazole forms 5-pyrazolide as a minor product. If the amount of 5-pyrazolide is significant relative to 1-pyrazolide in the SIFT-injected *m*/*z* 67 ions, then the kinetic measurements can be affected by the minor isomer. This issue is addressed below.

It is very difficult to accurately determine the proportion of 5-pyrazolide in *m*/*z* 67 ions from the observed photoelectron spectrum in Figure 1, because the relative cross sections of 1-pyrazolide and 5-pyrazolide, and their photoelectron kinetic energy dependences, are not known. We use the following procedure to evaluate the relative amount of 5-pyrazolide in the photoelectron spectroscopic measurements. We have recently measured photoelectron spectra of 1-methyl-5-pyrazolide ion.[43] The reaction of HO^- with 1-methylpyrazole generates the carbon-deprotonated ion; no deprotonation takes place at the N atom. The observed spectrum is composed of two parts. In the lower eBE region, detachment to the electronic ground state of 1-methyl-5-pyrazolyl radical ($^2A'$) is observed. At the higher eBE, the feature of the first excited state ($^2A''$) is observed with a lower intensity. The ratio of the integrated areas for the ground- and excited-state portions of the magic angle spectrum is about 4:1.[44] It should be noted that because detachment to the two states originates from the same ion, the ratio must represent the relative cross sections for the two states under the experimental conditions. The eKE relationship between the ground and excited states of 1-methyl-5-pyrazolyl radical is very similar to that between 5-pyrazolide and 1-pyrazolide. Furthermore, the detachment to the excited state of 1-methyl-5-pyrazolyl radical takes place from an anion π orbital, analogous to the detachment to 1-pyrazolyl. Therefore, it is reasonable to apply the ratio of the cross sections (∼4:1) to evaluate the relative abundance of 5-pyrazolide in Figure 1. In this way, 5-pyrazolide is estimated to account for 5% of the *m*/*z* 67 ions produced from HO^- deprotonation in the photoelectron spectroscopic apparatus.[45]

Since the ion source conditions in the FA-SIFT instrument are not exactly the same as those in the photoelectron spectroscopic apparatus, the relative abundance of 5-pyrazolide in the SIFT-injected *m*/*z* 67 ions should be evaluated independently. Acidity bracketing measurements were conducted for the SIFT-injected *m*/*z* 67 ions produced from the HO^- reaction with pyrazole in the source flow tube. The *m*/*z* 67 ions deprotonate $(CH_3)_3CSH$ ($\Delta_{acid}G_{298} = 346.2 \pm 0.2$ kcal mol^{-1})[8,22−24] efficiently, whereas deprotonation of CH_3SH ($\Delta_{acid}G_{298} = 351.6 \pm 0.4$ kcal mol^{-1})[7] is very slow. The DFT calculations predict the gas phase acidities of pyrazole to be $\Delta_{acid}G_{298} = 347.6$ kcal mol^{-1} for N1−H and 376.7 kcal mol^{-1} for C5−H. These results clearly indicate that the *m*/*z* 67 ions are predominantly 1-pyrazolide in the FA-SIFT instruments. The presence of a minor amount of 5-pyrazolide, however, was suggested from the kinetics of the *m*/*z* 67 ions that were SIFT-injected at different injection energies. When the *m*/*z* 67 ions were injected at an energy of 70 eV, deprotonation of CH_3SH was found to be slightly slower than when an energy of 20 eV was used. As shown in Figure 2, 5-pyrazolide is higher in energy than 1-pyrazolide by ∼30 kcal mol^{-1} according to the DFT calculations, and the 5-pyrazolide deprotonation of CH_3SH must be efficient. It is reasonable to assume that the more energetic 5-pyrazolide would be decomposed and lost at the higher injection energy of 70 eV, leaving the less basic 1-pyrazolide behind and making the overall deprotonation slower. Under this assumption, the upper limit for the proportion of 5-pyrazolide in the *m*/*z* 67 ions is estimated to be 6% at the 20 eV injection energy, which is consistent with the estimate based on the photoelectron spectra.

The presence of the minor 5-pyrazolide, however, does not affect our determination of the N−H gas phase acidity significantly. Unlike the 1-pyrazolide reaction with CH_3SH, the 1-pyrazolide reaction with $(CH_3)_3CSH$ (the forward reaction in eq 2) is exoergic. The rate constant of the forward reaction, $k_f = (1.08 \pm 0.22) \times 10^{-9}\ cm^3\ s^{-1}$, indicates that 1-pyrazolide deprotonates $(CH_3)_3CSH$ quite efficiently, fairly close to the calculated collision rate constant[19] of $1.83 \times 10^{-9}\ cm^3\ s^{-1}$ (the dipole moment[21] and the polarizability[20] of $(CH_3)_3CSH$ are 1.66 D and $11.2 \times 10^{-24}\ cm^3$, respectively). Therefore, although 5-pyrazolide is much more basic than 1-pyrazolide, its rate constant would not be much greater. Thus, the presence of 5-pyrazolide (<6%) could affect the rate constant only marginally, and the associated error bar is negligible compared to the stated error limits of 20% for the forward reaction. Indeed, no difference is found in the reactivity of the *m*/*z* 67 ions toward $(CH_3)_3CSH$ between the SIFT injection energies of 20 and 70 eV.

Discussion

Electronic Structure of 1-Pyrazolyl Radical. As mentioned in the Results section, the photoelectron spectrum of 1-pyrazolide demonstrates nonadiabatic effects in the low-lying electronic states of 1-pyrazolyl. This subject will be discussed in detail elsewhere,[10] so only a brief, qualitative account will be given here.

We have previously studied an isomeric system, 1-imidazolyl radical.[8] The electronic ground state of 1-imidazolyl has an unpaired electron located in a π orbital (b_1), which is composed mainly of p orbitals of C atoms. The second π orbital (a_2), on the other hand, has large contributions from p orbitals of N atoms, and it is much lower in energy than the b_1 orbital. Therefore, the second π state, $^2A_2$, where the unpaired electron resides in the a_2 orbital, is considerably higher in energy than the $\tilde{X}\ ^2B_1$ state. The large energy separation leads to only minor effects of vibronic interaction in the $\tilde{X}\ ^2B_1$ state around its equilibrium geometry.

With a different arrangement of the two N atoms in the five-membered ring, the energetic relation between two π orbitals in 1-pyrazolyl is quite different from that in 1-imidazolyl. Figure 6 illustrates photodetachment processes of 1-pyrazolide. Both a_2 and b_1 π orbitals of 1-pyrazolide have comparable contributions from the p orbitals of the two N atoms. Thus, the two π orbitals are energetically very close to each other, and the $^2A_2$ and $^2B_1$ states of 1-pyrazolyl, formed by electron detachment from the corresponding orbitals of 1-pyrazolide, are near-degenerate. Vibronic interaction of pseudo-Jahn−Teller type[46,47] between the two π states becomes significant even around the

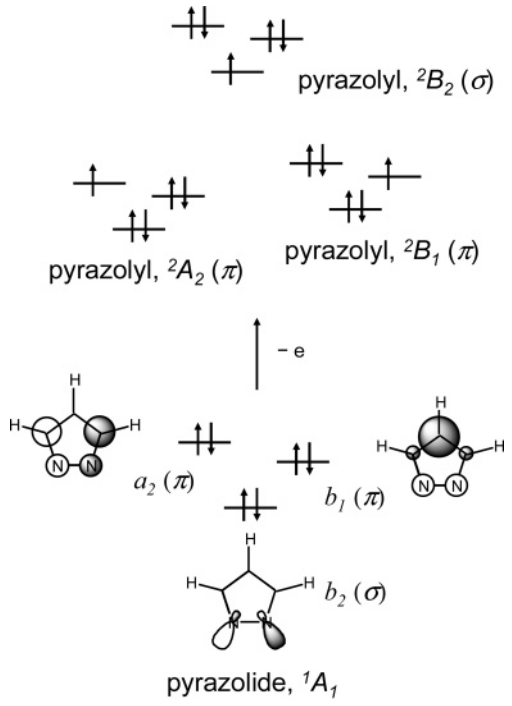

Figure 6. Schematic representation of photodetachment from 1-pyrazolide to form the low-lying electronic states of the 1-pyrazolyl radical. The three highest occupied molecular orbitals of 1-pyrazolide are depicted.

equilibrium geometries of both states. Therefore, FC simulation based on the Born−Oppenheimer approximation fails, as shown in Figure 4. The near-degeneracy might have prevented observation of a clear electron spin resonance (ESR) spectrum of 1-pyrazolyl radical in alkaline aqueous solution.[48] Further complications in vibronic interaction arise from the participation of yet another electronic state, $^2B_2$, as shown in Figure 6. This three-state interaction[49] in 1-pyrazolyl radical will be fully investigated in a forthcoming paper.[10]

Previously, it was discussed that successive replacements of CH units with N atoms in the five-membered ring lead to increases in the EA from cyclopentadienyl to pyrrolyl to imidazolyl.[8] Even though both 1-pyrazolyl and 1-imidazolyl have two N atoms in the ring, the EA of 1-pyrazolyl (2.938 ± 0.005 eV) is higher than that of 1-imidazolyl (2.613 ± 0.006 eV).[8] This difference reflects the character of the highest occupied molecular orbitals (HOMOs) for the anions; the HOMO of 1-pyrazolide has significant contributions from the p orbitals of the N atoms, while that of 1-imidazolide has only minor contributions. The HOMO of 1-pyrazolide is more stabilized, which results in the higher EA.

Pyrazole N−H Bond Thermodynamics. Our measurements of the EA of 1-pyrazolyl and the gas phase acidity of pyrazole allow us to determine the N−H bond dissociation energy (BDE) of pyrazole [D_0(pyrazole, N−H)] through a negative ion thermochemical cycle.

$$D_0(\text{pyrazole, N−H}) = \Delta_{\text{acid}}H_0(\text{pyrazole, N−H}) + \text{EA(1-pyrazolyl)} - \text{IE(H)} \quad (4)$$

Here, $\Delta_{\text{acid}}H_0$(pyrazole, N−H) is the 0 K N−H deprotonation enthalpy, EA(1-pyrazolyl) is the electron affinity of 1-pyrazolyl, and IE(H) is the ionization energy of the hydrogen atom (13.598 44 eV).[42] To obtain the 0 K N−H deprotonation enthalpy, the experimental 298 K gas phase acidity is first converted to the 298 K deprotonation enthalpy using $T\Delta_{\text{acid}}S_{298}$ evaluated from the DFT calculations; $\Delta_{\text{acid}}H_{298}$(pyrazole, N−H) = 353.6 ± 0.4 kcal mol^{-1}. The 298 K deprotonation enthalpy is subsequently converted to the 0 K deprotonation enthalpy using integrated heat capacities evaluated from the DFT calculations; $\Delta_{\text{acid}}H_0$(pyrazole, N−H) = 352.2 ± 0.4 kcal mol^{-1}. Then, eq 4 yields the N−H BDE, D_0(pyrazole, N−H) = 106.4 ± 0.4 kcal mol^{-1}.

TABLE 4: Thermochemical Parameters for Pyrazole and 1-Pyrazolyl

EA(1-pyrazolyl)[a]	2.938 ± 0.005 eV
$\Delta_{\text{acid}}G_{298}$(N−H)[a]	346.4 ± 0.3 kcal mol^{-1}
$\Delta_{\text{acid}}S_{298}$(N−H)[b]	24.2 cal mol^{-1} K^{-1}
$\Delta_{\text{acid}}H_{298}$(N−H)[c]	353.6 ± 0.4 kcal mol^{-1}
$\Delta_{\text{acid}}H_0$(N−H)[d]	352.2 ± 0.4 kcal mol^{-1}
D_0(N−H)[e]	106.4 ± 0.4 kcal mol^{-1}
Δ_fH_{298}(1-pyrazolyl)[f]	98.7 ± 0.5 kcal mol^{-1}

[a] Experimentally determined in the present study. [b] Derived from the B3LYP/6-311++G(d,p) calculations with vibrational frequencies unscaled. [c] Derived from $\Delta_{\text{acid}}G_{298}$ and $\Delta_{\text{acid}}S_{298}$. [d] Derived from $\Delta_{\text{acid}}H_{298}$ and the B3LYP/6-311++G(d,p) thermal corrections. [e] Determined from EA and $\Delta_{\text{acid}}H_0$ using a thermochemical cycle (eq 4 in the text). [f] Derived from Δ_fH_{298}(pyrazole) and D_0 with thermal corrections using eq 5 in the text.

The heat of formation of 1-pyrazolyl radical [Δ_fH(1-pyrazolyl)] can be determined through the following equation:

$$\Delta_fH_T(\text{1-pyrazolyl}) = \Delta_fH_T(\text{pyrazole}) + DH_T(\text{pyrazole, N−H}) - \Delta_fH_T(\text{H}) \quad (5)$$

where T designates the temperature. The 298 K heats of formation for pyrazole[50] and H atom[51] are available in the literature; Δ_fH_{298}(pyrazole) = 42.88 ± 0.20 kcal mol^{-1} and Δ_fH_{298}(H) = 52.1030 ± 0.0016 kcal mol^{-1}. The 298 K N−H bond enthalpy for pyrazole is derived from the N−H BDE using DFT thermal corrections; DH_{298}(pyrazole, N−H) = 108.0 ± 0.4 kcal mol^{-1}. With these values substituted, eq 5 yields Δ_fH_{298}(1-pyrazolyl) = 98.7 ± 0.5 kcal mol^{-1}. The DFT thermal correction has also been calculated for pyrazole to evaluate Δ_fH_0(pyrazole) = 46.8 ± 0.3 kcal mol^{-1}. With Δ_fH_0(H) = 51.6336 ± 0.0016 and the N−H BDE, Δ_fH_0(1-pyrazolyl) = 101.5 ± 0.5 kcal mol^{-1} is derived from eq 5. Table 4 summarizes the thermochemical data.

In our previous paper, it was noted that the N−H BDEs of pyrrole[52] (93.92 ± 0.11 kcal mol^{-1}) and imidazole[8] (95.1 ± 0.5 kcal mol^{-1}) are very close to each other, and rather insensitive to the number of N atoms in the ring. The N−H BDE of pyrazole, however, is much higher than that of imidazole. With respect to the thermochemical cycle, eq 4, the higher N−H BDE in pyrazole is a result of the higher EA and larger $\Delta_{\text{acid}}H_0$ value (i.e., lower acidity) on the right-hand side of eq 4, compared to imidazole.

The effect of an adjacent N atom on the N−H BDE of pyrazole contrasts with that in a nonaromatic system, hydrazine (N_2H_4). The N−H BDE of hydrazine has been determined to be 80.8 ± 0.3 kcal mol^{-1} from a photoionization mass spectroscopic study.[53] This N−H BDE is much lower than that of ammonia (NH_3), 106.12 ± 0.06 kcal mol^{-1}, determined from H Rydberg atom photofragment translational spectroscopy.[54] The much lower N−H BDE of N_2H_4 reflects three-electron stabilization of the hydrazyl radical (N_2H_3).[55] In hydrazine, there are two electrons in the bare sp^3 orbital of each N atom. The four electron interaction will not result in energy stabilization, so the two lone-pair orbitals are perpendicular to each other in hydrazine.[55,56] On the other hand, hydrazyl radical can stabilize

by the interaction of the bare (p) orbitals of the two N atoms because only three electrons need to be accommodated. This favorable interaction leads to a planar geometry for the radical with a partial π bonding. As a result, the NN bond in hydrazyl is much shorter than that in hydrazine.[55] It should be noted that the relatively low C−H BDEs for the C−H bonds adjacent to the N atoms in azines have been ascribed to the same three-electron stabilization mechanism in the in-plane orbital systems.[57,58]

Comparison between the N−H BDEs of pyrrole and pyrazole indicates that the presence of an adjacent N atom increases the N−H BDE in the five-membered aromatic systems. This opposite behavior reflects the fact that the unpaired electrons in the radicals formed by adiabatic N−H bond fission of pyrrole and pyrazole reside in the π orbitals. Thus, in $\tilde{X}\ ^2A_2$ 1-pyrazolyl radical, there is no three-electron stabilization because the lone-pair orbital of the adjacent N atom aligns itself along the molecular plane, perpendicular to the singly occupied π orbital. The three-electron stabilization can be seen instead in an excited state of 1-pyrazolyl, the $^2B_2$ state, where the NN bond length is much shorter than that in $\tilde{X}\ ^1A_1$ 1-pyrazolide, according to the DFT calculations (Table 1).

The opposite effects of the adjacent N atom on the N−H BDE have consequences in their reactivities. The rate constant of the OH radical reaction with hydrazine to form hydrazyl radical and H_2O is 4.5×10^9 M^{-1} s^{-1} in aqueous solution at room temperature.[59] This rate constant is much larger than that of the corresponding reaction for ammonia,[60] 9.7×10^7 M^{-1} s^{-1}. The same trend in reactivity has been found for these reactions in the gas phase.[61−64] The much larger rate constant for the H abstraction from hydrazine is in agreement with the weaker N−H bond in hydrazine, that is, the much larger exothermicity of the reaction (cf. the O−H BDE of H_2O is 117.66 ± 0.02 kcal mol^{-1}).[24,65] On the other hand, the OH radical reactions with pyrrole and pyrazole have a charge transfer character, involving the π electrons in the aromatic compounds, as discussed previously for the imidazole system.[8] The adjacent N atom makes pyrazole more resistant to π electron donation, as is evident in the EA of pyrazolyl (2.938 ± 0.005 eV) or the IE of pyrazole (9.15 eV),[66] both of which are much larger than the corresponding values for the pyrrole system[7,66] (EA 2.145 ± 0.010 eV and IE 8.23 eV). Thus, pyrrolyl radical is relatively easily formed in the OH + pyrrole reaction in neutral aqueous solution, while the formation of pyrazolyl radical from the OH + pyrazole reaction requires base catalysis in alkaline solution.[48]

The gas phase acidity value of pyrazole determined in this study (346.4 ± 0.3 kcal mol^{-1}) is in good agreement with a reported value (346.4 ± 2.0 kcal mol^{-1}), but our measurement has a much smaller error bar because of the reduced uncertainty in the acidity of the reference acid, $(CH_3)_3CSH$.[8,22−24] The difference in the acidity between pyrazole and imidazole has been discussed in the literature with respect to the electrostatic interaction between two N atoms in the ring.[40]

Electronic Structure of 5-Pyrazolyl Radical. The observed photoelectron spectrum of 5-pyrazolide (Figure 5) bears some similarity with that of 5-imidazolide.[8] The EA of 5-pyrazolyl is 2.104 ± 0.005 eV, close to that of 5-imidazolyl, 1.992 ± 0.010 eV.[8] The 5-pyrazolide spectrum exhibits an extensive vibrational progression along an in-plane ring bending mode, which is also observed in the 5-imidazolide spectrum. In both anions, the HOMO is an in-plane (σ) orbital, mainly localized on the C5 atom. Detachment from this orbital affects the interior angles of the pentagon, particularly one centered at C5 (Table 3).

Another comparison can be made with the photoelectron spectrum of phenide anion.[67] The phenide spectrum also displays extensive vibrational progressions along two in-plane ring bending modes both of which involve the angle centered at the deprotonated C atom.[68] The EA of phenyl radical,[67] 1.096 ± 0.006 eV, however, is much lower than those of 5-pyrazolyl and 5-imidazolyl. Two factors can cause the differences in the EAs. First, the σ HOMO of 5-pyrazolide (or 5-imidazolide) is significantly stabilized by electronic interaction with the N atomic orbitals, which are absent in phenide. Second, the C4−C5−N1 angle of the 5-pyrazolide (or 5-imidazolide) ground state is substantially smaller than the corresponding CCC angle for phenide.[67] Thus, there is more contribution of the s orbital of the C5 atom in the σ HOMO of 5-pyrazolide (or 5-imidazolide), making it more stable than the σ HOMO of phenide.

The positive anisotropy parameter (β) found for 5-pyrazolide photoelectrons in the eKE region of 0.8−1.5 eV is reminiscent of the positive β value observed for the photoelectron spectrum of phenide in the eKE region of 1.5−2.5 eV.[67] This positive β value may be a signature of detachment from σ orbitals of aromatic systems in the low-eKE range.

Pyrazole C−H Bond Thermodynamics. Successful FC simulation of the photoelectron spectrum in Figure 5 confirms that HO^- deprotonates pyrazole at the C5 position. The DFT calculations predict $\Delta_{acid}G_{298}$ = 391.7, 388.9, and 376.7 kcal mol^{-1} for the pyrazole acidity at the C3, C4, and C5 positions, respectively. Since $\Delta_{acid}G_{298}$ = 383.68 ± 0.02 kcal mol^{-1} for H_2O,[24] the DFT calculations are consistent with our experimental finding that only 5-pyrazolide among carbon-deprotonated species was observed from the reaction of HO^- with pyrazole (see also Figure 2). It is notable that DFT predicts $\Delta_{acid}G_{298}$ = 347.6 kcal mol^{-1} for the N−H site of pyrazole, which is in good agreement with our experimental value, 346.4 ± 0.3 kcal mol^{-1}.

No formation of 5-pyrazolide has been observed in our photoelectron spectroscopic measurements when O^- or F^- is the reactant for pyrazole. The gas phase acidities of hydroxyl radical[29] and hydrogen fluoride[24] are 376.69 ± 0.07 and 365.577 ± 0.003 kcal mol^{-1}, respectively. Thus, our photoelectron measurements suggest that the gas phase acidity of pyrazole at the C5 position is bracketed between H_2O and OH radical; $\Delta_{acid}G_{298}$(pyrazole, C5−H) = 380 ± 4 kcal mol^{-1}. Analogous to the N−H system treated in a previous section, the pyrazole C5−H BDE can be derived as D_0(pyrazole, C5−H) = 121 ± 4 kcal mol^{-1} from a thermochemical cycle, similar to eq 4, but for the C5−H bond.

Our previous photoelectron spectroscopic study has found that the hydrogen at the C5 position of imidazole is the most acidic among all of the C−H sites in imidazole.[8] The relatively acidic C5 hydrogen of imidazole has been attributed to the effects of an adjacent N−H group and an N atom at the β position.[8,40] The C5−H of pyrazole also has an adjacent N−H group and a β N atom. This situation makes pyrazole more acidic at the C5 position than at the C3 or C4 position. It should be noted that, following HO^- deprotonation, the spectrum of 5-pyrazolide appears much more intense than that of 5-imidazolide relative to the corresponding 1-azolide spectra. Using the DFT acidity values and the reported $\Delta_{acid}G_{298}(H_2O)$ value,[24] the free energy changes for the HO^- reaction with pyrazole and imidazole to form 5-pyrazolide and 5-imidazolide, respectively, are evaluated to be −6.9 and −3.5 kcal mol^{-1}. Thus, the experimental observations may indicate that the C5 site of pyrazole is more acidic than the C5 site of imidazole.

Conclusion

The photoelectron spectrum of 1-pyrazolide has been measured, and the EA of 1-pyrazolyl is determined to be 2.938 ± 0.005 eV. The gas phase acidity of pyrazole is determined to be $\Delta_{acid}G_{298} = 346.4 \pm 0.3$ kcal mol^{-1} from the proton transfer rate constant measurements for the pyrazole−$(CH_3)_3CSH$ system. These thermodynamic parameters are used in a thermochemical cycle to derive the N−H BDE of pyrazole to be D_0(pyrazole, N−H) = 106.4 ± 0.4 kcal mol^{-1}. The photoelectron spectrum of 1-pyrazolide indicates nonadiabatic effects in the low-lying states of 1-pyrazolyl. Our detailed analysis of the vibronic structure of the 1-pyrazolyl states will be given in a separate paper.[10] The HO^- deprotonation of pyrazole yields a minor product ion, 5-pyrazolide, as identified from the FC fitting of the photoelectron spectrum of the minor ion based on the results of the B3LYP/6-311++G(d,p) calculations. The EA of 5-pyrazolyl radical is 2.104 ± 0.005 eV. Fundamental vibrational frequencies of 890 ± 15, 1110 ± 35, and 1345 ± 30 cm^{-1} have been assigned to an in-plane CCN bending mode and two in-plane ring bond-stretching modes, respectively, of $\tilde{X}\ ^2A'$ 5-pyrazolyl. An extensive vibrational progression along the CCN bending mode is evident in the spectrum, suggesting a substantial change in the CCN angle from the anion to the neutral ground states. The formation of 5-pyrazolide is not observed in the O^- or F^- reactions with pyrazole in the photoelectron spectroscopic measurements. Using the gas phase acidities of H_2O and OH radical, the gas phase acidity of pyrazole at the C5 position is evaluated to be $\Delta_{acid}G_{298}$(pyrazole, C5−H) = 380 ± 4 kcal mol^{-1} by bracketing. A thermochemical cycle is employed to evaluate the C5−H BDE of pyrazole as D_0(pyrazole, C5−H) = 121 ± 4 kcal mol^{-1}. The relatively large error bar arises from the uncertainty in the acidity of pyrazole at the C5 position. We have recently measured the gas phase acidity of 1-methylpyrazole and the EA of 1-methyl-5-pyrazolyl radical to determine the C5−H BDE of 1-methylpyrazole very accurately.[43] Information on the C−H BDE of five-membered heterocyclic compounds is useful for understanding combustion processes[58,69−72] and transition-metal catalysis.[73−79]

We have completed studies of five-membered, heterocyclic compounds that contain up to two N atoms in the ring. We have recently initiated an investigation of the thermochemical properties of the triazole system (i.e., three N atoms in the ring), which will be presented in a forthcoming paper.[80]

Acknowledgment. We are grateful to Professor John F. Stanton for elucidation of the vibronic coupling effects in the 1-pyrazolyl radical. We are pleased to acknowledge helpful discussion with Ms. Stephanie M. Villano. This work was supported by the Air Force Office of Scientific Research and by the National Science Foundation (grants CHE-0349937 and CHE-0512188).

Supporting Information Available: Tables showing the B3LYP/6-311++G(d,p) harmonic vibrational frequencies for 1-pyrazolide, 1-pyrazolyl, 5-pyrazolide, and 5-pyrazolyl. This material is available free of charge via the Internet at http://pubs.acs.org.

References and Notes

(1) Klapotke, T. M. *Angew. Chem., Int. Ed.* **1999**, *38*, 2536−2538.
(2) Hammerl, A.; Klapotke, T. M. *Inorg. Chem.* **2002**, *41*, 906−912.
(3) Nguyen, M. T. *Coord. Chem. Rev.* **2003**, *244*, 93−113.
(4) Kwon, O.; McKee, M. L. In *Energetic Materials, Part 1: Decomposition, Crystal and Molecular Properties*; Politzer, P., Murray, J. S., Eds.; Elsevier: Amsterdam, The Netherlands, 2003; pp 405−420.
(5) Brinck, T.; Bittererova, M.; Ostmark, H. In *Energetic Materials, Part 1: Decomposition, Crystal and Molecular* Properties; Politzer, P., Murray, J. S., Eds.; Elsevier: Amsterdam, The Netherlands, 2003; pp 421−439.
(6) Fau, S.; Bartlett, R. J. In *Energetic Materals, Part 1: Decomposition, Crystal and Molecular Properties*; Politzer, P., Murray, J. S., Eds.; Elsevier: Amsterdam, The Netherlands, 2003; pp 441−455.
(7) Gianola, A. J.; Ichino, T.; Hoenigman, R. L.; Kato, S.; Bierbaum, V. M.; Lineberger, W. C. *J. Phys. Chem. A* **2004**, *108*, 10326−10335.
(8) Gianola, A. J.; Ichino, T.; Hoenigman, R. L.; Kato, S.; Bierbaum, V. M.; Lineberger, W. C. *J. Phys. Chem. A* **2005**, *109*, 11504−11514.
(9) In our previous publications (refs 7 and 8), pyrrolide (or pyrrolyl) and imidazolide (or imidazolyl) were used interchangeably with 1-pyrrolide (or 1-pyrrolyl) and 1-imidazolide (or 1-imidazolyl), respectively. In the present paper, we make the position of deprotonation explicit in nomenclature to avoid confusion.
(10) Gianola, A. J.; Ichino, T.; Lineberger, W. C.; Stanton, J. F. Manuscript to be published.
(11) Ervin, K. M.; Lineberger, W. C. In *Advances in Gas Phase Ion Chemistry*; Adams, N. G., Babcock, L. M., Eds.; JAI Press: Greenwich, CT, 1992; Vol. 1, pp 121−166.
(12) Leopold, D. G.; Murray, K. K.; Stevens-Miller, A. E.; Lineberger, W. C. *J. Chem. Phys.* **1985**, *83*, 4849.
(13) Ervin, K. M.; Ho, J.; Lineberger, W. C. *J. Chem. Phys.* **1989**, *91*, 5974.
(14) Andersen, T.; Haugen, H. K.; Hotop, H. *J. Phys. Chem. Ref. Data* **1999**, *28*, 1511−1533.
(15) Rienstra-Kiracofe, J. C.; Tschumper, G. S.; Schaefer, H. F.; Nandi, S.; Ellison, G. B. *Chem. Rev.* **2002**, *102*, 231−282.
(16) Cooper, J.; Zare, R. N. *J. Chem. Phys.* **1968**, *48*, 942−943.
(17) Van Doren, J. M.; Barlow, S. E.; DePuy, C. H.; Bierbaum, V. M. *Int. J. Mass Spectrom. Ion Processes* **1987**, *81*, 85−100.
(18) Bierbaum, V. M. In *Encyclopedia of Mass Spectrometry*: *Theory and Ion Chemistry*; Gross, M. L., Caprioli, R., Eds.; Elsevier: Amsterdam, The Netherlands, 2003; Vol. 1, pp 276−292.
(19) Su, T.; Chesnavich, W. J. *J. Chem. Phys.* **1982**, *76*, 5183−5185.
(20) Miller, K. J.; Savchik, J. A. *J. Am. Chem. Soc.* **1979**, *101*, 7206−7213.
(21) *CRC Handbook of Chemistry and Physics*, 86th ed.; Lide, D. R., Ed.; CRC Press: Boca Raton, FL, 2005.
(22) Bartmess, J. E.; Scott, J. A.; McIver, R. T. *J. Am. Chem. Soc.* **1979**, *101*, 6046−6056.
(23) Shiell, R. C.; Hu, X. K.; Hu, Q. J.; Hepburn, J. W. *J. Phys. Chem. A* **2000**, *104*, 4339−4342.
(24) Ervin, K. M.; DeTuro, V. F. *J. Phys. Chem. A* **2002**, *106*, 9947−9956.
(25) Becke, A. D. *J. Chem. Phys.* **1993**, *98*, 5648−5652.
(26) Lee, C. T.; Yang, W. T.; Parr, R. G. *Phys. Rev. B* **1988**, *37*, 785−789.
(27) Krishnan, R.; Binkley, J. S.; Seeger, R.; Pople, J. A. *J. Chem. Phys.* **1980**, *72*, 650−654.
(28) Frisch, M. J.; Trucks, G. W.; Schlegel, H. B.; Scuseria, G. E.; Robb, M. A.; Cheeseman, J. R.; Montgomery, J. A., Jr.; Vreven, T.; Kudin, K. N.; Burant, J. C.; Millam, J. M.; Iyengar, S. S.; Tomasi, J.; Barone, V.; Mennucci, B.; Cossi, M.; Scalmani, G.; Rega, N.; Petersson, G. A.; Nakatsuji, H.; Hada, M.; Ehara, M.; Toyota, K.; Fukuda, R.; Hasegama, J.; Ishida, M.; Nakajima, T.; Honda, Y.; Kitao, O.; Nakai, H.; Klene, M.; Li, X.; Knox, J. E.; Hratchian, H. P.; Cross, J. B.; Adamo, C.; Jaramillo, J.; Gomperts, R.; Stratmann, R. E.; Yazyev, O.; Austin, A. J.; Cammi, R.; Pomelli, C.; Ochterski, J. W.; Ayala, P. Y.; Morokuma, K.; Voth, G. A.; Salvador, P.; Dannenberg, J. J.; Zakrzewski, V. G.; Dapprich, S.; Daniels, A. D.; Strain, M. C.; Farkas, O.; Malick, D. K.; Rabuck, A. D.; Raghavachari, K.; Foresman, J. B.; Ortiz, J. V.; Cui, Q.; Baboul, A. G.; Clifford, S.; Cioslowski, J.; Stefanov, B. B.; Liu, G.; Liashenko, A.; Piskorz, P.; Komaromi, I.; Martin, R. L.; Fox, D. J.; Keith, T.; Al-Laham, M. A.; Peng, C. Y.; Nanayakkara, A.; Challacombe, M.; Gill, P. M. W.; Johnson, B.; Chen, W.; Wong, M. W.; Gonzalez, C.; Pople, J. A. *Gaussian 03*, revision B.05; Gaussian, Inc.: Pittsburgh, PA, 2003.
(29) Ruscic, B.; Wagner, A. F.; Harding, L. B.; Asher, R. L.; Feller, D.; Dixon, D. A.; Peterson, K. A.; Song, Y.; Qian, X. M.; Ng, C. Y.; Liu, J. B.; Chen, W. W. *J. Phys. Chem. A* **2002**, *106*, 2727−2747.
(30) Ervin, K. M. *PESCAL, Fortran program*; http://www.chem.unr.edu/~ervin/pes; University of Nevada, Reno: Reno, NV, 2003.
(31) Ervin, K. M.; Ramond, T. M.; Davico, G. E.; Schwartz, R. L.; Casey, S. M.; Lineberger, W. C. *J. Phys. Chem. A* **2001**, *105*, 10822−10831.
(32) Only totally symmetric modes are considered in the Franck−Condon overlap calculations.
(33) The photoelectron kinetic energy dependence of the detachment cross section has only minor effects on the relative peak intensities. Also, for the energy range in Figure 4 (eBE < 3.2 eV or eKE > 0.3 eV), there should not be any significant instrumental artifacts on the relative peak intensities.

(34) Koppel, H.; Domcke, W.; Cederbaum, L. S. *Adv. Chem. Phys.* **1984**, *57*, 59−246.
(35) Bomble, Y. J.; Sattelmeyer, K. W.; Stanton, J. F.; Gauss, J. *J. Chem. Phys.* **2004**, *121*, 5236−5240.
(36) Hazra, A.; Nooijen, M. *Phys. Chem. Chem. Phys.* **2005**, *7*, 1759−1771.
(37) Stanton, J. F.; Gauss, J. *J. Chem. Phys.* **1994**, *101*, 8938−8944.
(38) Stanton, J. F. *J. Chem. Phys.* **2001**, *115*, 10382−10393.
(39) This scaling factor is very similar to a standard scaling factor used for the B3LYP method with a similar basis set. Scott, A. P.; Radom, L *J. Phys. Chem.* **1996**, *100*, 16502.
(40) Taft, R. W.; Anvia, F.; Taagepera, M.; Catalan, J.; Elguero, J. *J. Am. Chem. Soc.* **1986**, *108*, 3237−3239.
(41) Catalan, J.; Claramunt, R. M.; Elguero, J.; Laynez, J.; Menendez, M.; Anvia, F.; Quian, J. H.; Taagepera, M.; Taft, R. W. *J. Am. Chem. Soc.* **1988**, *110*, 4105−4111.
(42) NIST Standard Reference Database Number 69, June 2005 Release.
(43) Villano, S. M.; Gianola, A. J.; Ichino, T.; Kato, S.; Bierbaum, V. M.; Lineberger, W. C. Manuscript to be published.
(44) The relatively small cross section of the detachment to the excited state of 1-methyl-5-pyrazolyl radical is consistent with the findings for 5-pyrazolyl. The DFT calculations predict that the term energy of the lowest excited state of 5-pyrazolyl (^{2}A″) is 0.772 eV. Combined with the EA of 5-pyrazolyl, DFT predicts the origin of the ^{2}A″ state to appear at eBE ∼2.88 eV. This eBE corresponds to the hot band region of the 1-pyrazolide spectrum (Figure 1). We have conducted Franck−Condon simulation for the ^{2}A″ state, and we do not recognize any feature observed at eBE > 2.8 eV in Figure 1 (or Figure 3) assignable to the 5-pyrazolyl excited state.
(45) A factor of 2 was taken into account because there are two electronic states apparent in the 1-pyrazolide spectrum.
(46) Pearson, R. G. *J. Am. Chem. Soc.* **1969**, *91*, 4947−4955.
(47) Fischer, G. *Vibronic Coupling*; Academic Press: London, 1984.
(48) Samuni, A.; Neta, P. *J. Phys. Chem.* **1973**, *77*, 1629−1635.
(49) Matsika, S.; Yarkony, D. R. *J. Am. Chem. Soc.* **2003**, *125*, 12428−12429.
(50) Jimenez, P.; Roux, M. V.; Turrion, C.; Gomis, F. *J. Chem. Thermodyn.* **1987**, *19*, 985−992.
(51) Chase, J., M. W. *NIST-JANAF Thermochemical Tables*, 4th ed.; American Chemical Society: Washington, DC, 1998.
(52) Cronin, B.; Nix, M. G. D.; Qadiri, R. H.; Ashfold, M. N. R. *Phys. Chem. Chem. Phys.* **2004**, *6*, 5031−5041.
(53) Ruscic, B.; Berkowitz, J. *J. Chem. Phys.* **1991**, *95*, 4378−4384.
(54) Mordaunt, D. H.; Dixon, R. N.; Ashfold, M. N. R. *J. Chem. Phys.* **1996**, *104*, 6472−6481.
(55) Armstrong, D. A.; Yu, D.; Rauk, A. *J. Phys. Chem. A* **1997**, *101*, 4761−4769.
(56) Kohata, K.; Fukuyama, T.; Kuchitsu, K. *J. Phys. Chem.* **1982**, *86*, 602−606.
(57) Kiefer, J. H.; Zhang, Q.; Kern, R. D.; Yao, J.; Jursic, B. *J. Phys. Chem. A* **1997**, *101*, 7061−7073.
(58) Barckholtz, C.; Barckholtz, T. A.; Hadad, C. M. *J. Am. Chem. Soc.* **1999**, *121*, 491−500.
(59) Buxton, G. V.; Stuart, C. R. *J. Chem. Soc., Faraday Trans.* **1996**, *92*, 1519−1525.
(60) Hickel, B.; Sehested, K. *Radiat. Phys. Chem.* **1992**, *39*, 355−357.
(61) Atkinson, R.; Baulch, D. L.; Cox, R. A.; Hampson, R. F.; Kerr, J. A.; Rossi, M. J.; Troe, J. *J. Phys. Chem. Ref. Data* **1997**, *26*, 1329−1499.
(62) Vaghjiani, G. L. *Int. J. Chem. Kinet.* **2001**, *33*, 354−362.
(63) The mechanisms of these gas phase reactions have been theoretically studied. See ref 55 and Basch, H.; Hoz, S. *J. Phys. Chem. A* **1997**, *101*, 4416−4431.
(64) The difference in the mechanism of the OH radical reaction with hydrazine between the gas phase and aqueous solution has been discussed in refs 55 and 62.
(65) Harich, S. A.; Hwang, D. W. H.; Yang, X. F.; Lin, J. J.; Yang, X. M.; Dixon, R. N. *J. Chem. Phys.* **2000**, *113*, 10073−10090.
(66) Cradock, S.; Findlay, R. H.; Palmer, M. H. *Tetrahedron* **1973**, *29*, 2173−2181.
(67) Gunion, R. F.; Gilles, M. K.; Polak, M. L.; Lineberger, W. C. *Int. J. Mass Spectrom. Ion Processes* **1992**, *117*, 601−620.
(68) In ref 67, the assignment of one of the two active modes in the photoelectron spectrum of phenide ion is not definitive. Our Franck−Condon simulation with the B3LYP/6-311++G(d,p) calculations unequivocally indicates that the other active mode (968 cm^{-1}) is another in-plane ring bending mode.
(69) Mackie, J. C.; Colket, M. B.; Nelson, P. F.; Esler, M. *Int. J. Chem. Kinet.* **1991**, *23*, 733−760.
(70) Bacskay, G. B.; Martoprawiro, M.; Mackie, J. C. *Chem. Phys. Lett.* **1998**, *290*, 391−398.
(71) Zhai, L.; Zhou, H. F.; Liu, R. F. *J. Phys. Chem. A* **1999**, *103*, 3917−3922.
(72) Hore, N. R.; Russell, D. K. *New J. Chem.* **2004**, *28*, 606−613.
(73) Jones, W. D.; Feher, F. J. *Acc. Chem. Res.* **1989**, *22*, 91−100.
(74) Jones, W. D.; Dong, L. Z.; Myers, A. W. *Organometallics* **1995**, *14*, 855−861.
(75) Musaev, D. G.; Morokuma, K. *J. Am. Chem. Soc.* **1995**, *117*, 799−805.
(76) Arndtsen, B. A.; Bergman, R. G.; Mobley, T. A.; Peterson, T. H. *Acc. Chem. Res.* **1995**, *28*, 154−162.
(77) Vigalok, A.; Uzan, O.; Shimon, L. J. W.; Ben-David, Y.; Martin, J. M. L.; Milstein, D. *J. Am. Chem. Soc.* **1998**, *120*, 12539−12544.
(78) Rybtchinski, B.; Cohen, R.; Ben-David, Y.; Martin, J. M. L.; Milstein, D. *J. Am. Chem. Soc.* **2003**, *125*, 11041−11050.
(79) Wiley: J. S.; Oldham, W. J.; Heinekey, D. M. *Organometallics* **2000**, *19*, 1670−1676.
(80) Andrews, D. H.; Rathbone, G. J.; Misaizu, F.; Calvi, R. M. D.; Lineberger, W. C. Manuscript to be published.